3-2008

Ultrafast Spectroscopy of Mid-Infrared Semiconductors Using the Signal and Idler Beams of a Synchronous Optical Parametric Oscillator

Richard M. Derbis

Ultrafast spectroscopy of mid-infrared semiconductors using the signal and idler beams of a synchronous optical parametric oscillator

THESIS

Richard M. Derbis, Captain, USAF

AFIT/GAP/ENP/08-M02

DEPARTMENT OF THE AIR FORCE
AIR UNIVERSITY

AIR FORCE INSTITUTE OF TECHNOLOGY

Wright-Patterson Air Force Base, Ohio

The views expressed in this thesis are those of the author and do not reflect the official policy or position of the United States Air Force, Department of Defense, or the United States Government.

AFIT/GAP/ENP/08-M02

Ultrafast spectroscopy of mid-infrared semiconductors using the signal and idler beams of a synchronous optical parametric oscillator

THESIS

Presented to the Faculty

Department of Engineering Physics

Graduate School of Engineering and Management

Air Force Institute of Technology

Air University

Air Education and Training Command

In Partial Fulfillment of the Requirements for the

Degree of Master of Science

Richard M. Derbis, BS

Captain, USAF

March 2008

AFIT/GAP/ENP/08-M02

Ultrafast spectroscopy of mid-infrared semiconductors using the signal and idler beams of a synchronous optical parametric oscillator

Richard M. Derbis, BS
Captain, USAF

Approved:

/signed/	March 2008
Michael A. Marciniak (Chairman)	Date
/signed/	March 2008
Robert L. Hengehold (Member)	Date
/signed/	March 2008
David E. Weeks (Member)	Date

AFIT/GAP/ENP/08-M02

Abstract

Mid-Wave Infrared (MWIR) semiconductors are of use to the Air Force for several applications. Ultrafast spectroscopy can be used to better quantify the effectiveness of semiconductor opto-electronic devices. The objective of this thesis was to improve the procedure for taking ultrafast, time-resolved measurements of photoluminescence from MWIR semiconductors. Previous work has used a mode-locked titanium sapphire (Ti:Saph) laser to excite the semiconductor sample and to upconvert the photoluminescence from the semiconductor. Work completed in this thesis improved on the techniques developed during previous work. A synchronous Optical Parameter Oscillator (OPO) will be used to convert the Ti:Saph laser (0.830 μm) into 1.3-μm signal and 2.3-μm idler beams. Whereas the Ti:Saph reference and signal beams were too energetic to excite the quantum well (QW) layers of certain MWIR opto-electronic semiconductor structures, the synchronous OPO allows investigation of the active layer by directly exciting the QWs. Photoluminescence was detected from an indium arsenide antimonide (InAsSb) sample with a peak wavelength of 3.8 μm. A detailed procedure for setup of the TRPL experiment using the synchronous OPO is provided.

Acknowledgements

I would like to thank all those who helped me during my time at AFIT. My time here has been a learning experience that I would never have received without the United States Air Force's aid. With the help of my professors and classmates, I have learned much about myself as a student and an officer.

I am grateful for Dr. Marcinak's patience and experience in giving me guidance when encountering problems in the lab. I would like to thank Mike Ranft and Greg Smith for taking their time to help with equipment issues.

Above all I am thankful to have such a loving and understanding wife. Even as she worked on her M.S. at AFIT, she still took the time to read my thesis. I can not thank her enough for her support during this difficult time.

Richard M. Derbis

Table of Contents

Page

List of Figures

List of Tables

List of Abbreviations

Ultrafast spectroscopy of mid-infrared semiconductors using the signal and idler beams of a synchronous optical parametric oscillator

I. Introduction

With the introduction of the FIM-92 Stinger (Redeye II) by General Dynamics in 1967 [16], there has been a persistant threat of a man-portable air defense system (MANPADs) attack against military and civilian aircraft. To ensure the safety of U.S. civilians and military personnel, a method of deterring, detecting and defeating these infrared (IR) based systems is needed.

Currently, it is estimated that there are over 700,000 [11] active MANPADs in the world, with between 50,000 to 100,000 [4] available to non-government agencies. The cost of a single unit is between $35,000 and $200,000 [9], making them easily attainable by extremist groups.

As a result of the threat of these IR systems, work has been done to reduce the proliferation of these threats and their use specifically to civilian aircraft. [18, 19, 25] Two methods that have been used to reduce the threat have been purchasing the outstanding arms to deter use and using flares to defeat them.

Traditional countermeasure methods against IR systems have been employing Magnesium-Teflon-Viton (MTV) flares. These flares work by deploying a pyrophoric material that ignites in contact with air. Since the pyrophoric material is hazardous, a suitable alternative is required. Also, MTV flare decoys have been suitable for first generation surface-to-air missiles (SAMs), such as the SA-7, but lack the ability to counter second generation SAMs. [5] First generation missiles used a single IR frequency to acquire a target. This acquisition method could be fooled by the MTVs. Current IR threats acquire their target using two frequencies, only one of which is

in the IR. The second signal is detected in the ultra-violet (UV) region. MTV flares have a low success rate against current IR missiles because of the UV frequency used to supplement target acquisition.

1.1 Motivation

Two current technologies are being investigated to defeat IR threats. They are the U.S. Army's Advanced Threat Infrared Countermeasure (ATIRCM) and the U.S. Special Operations Command's Directional Infrared Countermeasure (DIRCM). [17] These systems employ IR lasers broadcasting several jamming algorithms intended to confuse an incoming missile. The current challenge is to build smaller and more powerful lasers. One such program underway is the Defense Advanced Research Projects Agency's (DARPA) Steered Agile Beam (STAB). STAB's goal is to develop a higher power IR laser and a faster moving tracking and engagement pod. [13]

Interband IR semiconductor lasers operate using the decay of excited electrons from the conduction band of a semiconductor to the valence band. This decay results in a source of Mid-Wave Infrared (MWIR) radiation. Since heat signatures from aircraft naturally broadcast in this window, MWIR sources are ideal for defense use. They are usable in an atmospheric electromagnetic transmission window (2-5 μm). Figure 1.1 shows the transmittance of wavelengths up to 15 μm in the atmosphere. As seen in Figure 1.1, UV lasers are impractical as a countermeasure due, in part, to large absorption in the atmosphere by water molecules.

The needs for our aircraft to be protected from hostile munitions, and for our munitions to be assured of hitting their target, means the development of IR based counter and counter-counter measures are interests of national security. It is these needs that are driving current programs investigating and developing MWIR opto-electric devices.

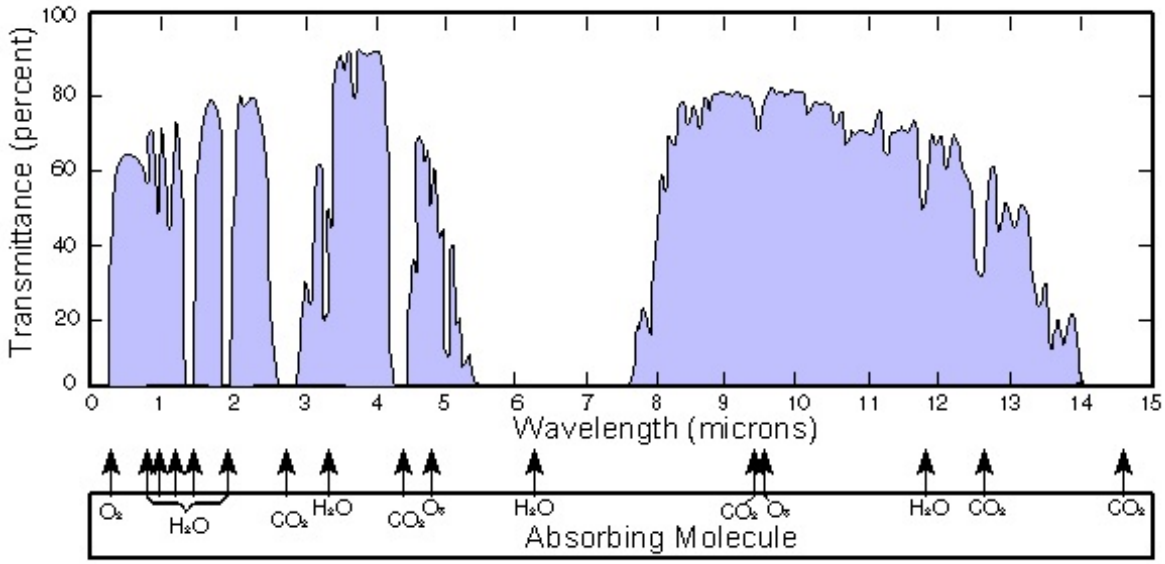

Figure 1.1. Graph of atmospheric transmittance for wavelengths up to 15 μm [1]

1.2 Background

A better understanding of MWIR structures will aid in the development of higher power IR lasers. Three areas that will be explored a bit here and in greater depth in Chapter 2 are the rate equation, photoluminescence (PL) and time-resolved photoluminescence (TRPL). The rate equation describes the decay of electrons from the conduction band to the valence band within a MWIR semiconductor structure. PL is the term for the light emitted in this decay when the electrons are excited by optical radiation. TRPL is the process that will be used to study PL.

1.2.1 Rate Equation. For bulk semiconductors, carrier dynamics can be described by the rate equation

$$\frac{1}{\tau} = \frac{\delta R}{\delta n} \tag{1.1}$$

where τ is the differential carrier lifetime, R is the recombination rate and n is the excited carrier density. A power series solution can be assumed for R of the form

$$R(n) = \sum_{i=0}^{\infty} A_i n^i. \tag{1.2}$$

Substituting Equation (1.2) into (1.1) yields

$$\frac{1}{\tau} = \sum_{i=1}^{\infty} A_i n^{i-1}. \tag{1.3}$$

An expansion of Equation (1.3) would involve an infinite number of terms and would be impossible to fit to for any computer. As a result, the generally accepted method of dealing with this problem is to truncate all but the first three terms and to assume all other terms are negligible in comparison. This assumption leads to

$$-\frac{dn}{dt} = A \cdot n + B \cdot n^2 + C \cdot n^3. \tag{1.4}$$

This is the rate equation for recombination within a semiconductor. The coefficients A, B and C are related to the probability of relaxation.

1.2.2 Photoluminescence. PL is light emitted by a sample following the absorption of optical photons. It occurs when an electron is excited to a higher energy level by absorbing a photon, and then spontaneously decays to a lower energy level, emitting a second photon in the process. To conserve energy, the emitted photon cannot have more energy than the exciting photon. [21]

1.2.3 Time Resolved Photoluminescence. TRPL is a procedure that will be used to study the PL produced by a semiconductor. It involves a second non-collinear laser beam to sample the PL. Using a nonlinear crystal, the sample beam can combine with the PL through nonlinear effects; this combination is called upconversion. Figure 1.2 shows how a sample beam combines with the PL to yield a third beam.

When the sampling beam is pulsed, time resolution is possible. Using a pulsed laser, the PL can be sampled at varying times. Figure 1.3 shows how this is accomplished. A pulse at t=0 excites the semiconductor which then begins to luminesce. The intensity can then be resolved temporally by delaying the sampling pulse. To determine the time at which t=0, it is necessary to find zero path length (ZPL). ZPL

is defined as the path length difference between the sampling pulse and the excitation pulse/PL such that the start of the excitation pulse/PL overlaps with the sampling pulse in the nonlinear crystal.

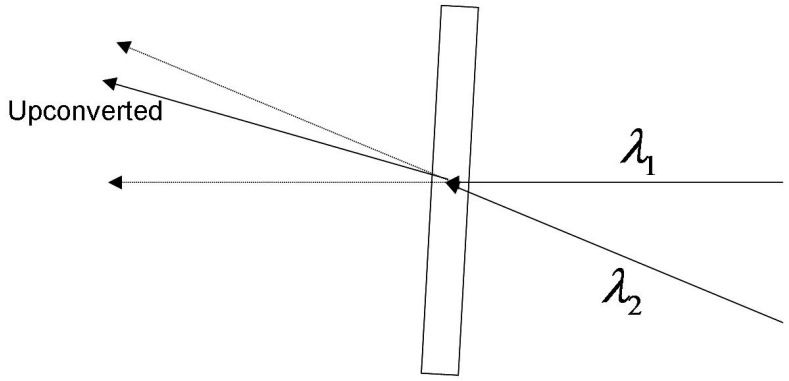

Figure 1.2. A diagram of upconversion. Two input beams enter the nonlinear crystal from the right and result in a third upconverted beam on the left. The beams above and below the upconverted beam are the input beams if there is no upconversion. Due to conservation of momentum the resultant beam will be able to be separated from the PL and sample beam components.

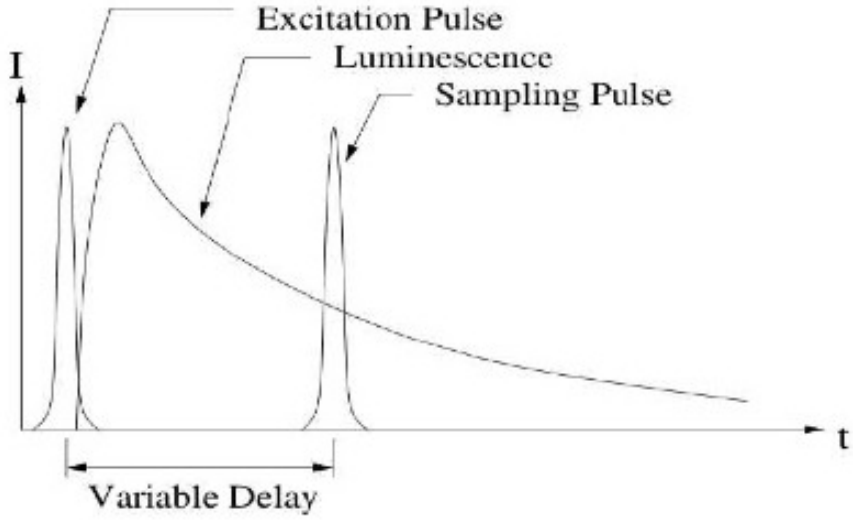

Figure 1.3. A diagram of TRPL. A pulse at t=0 excites the semicondutor, which then begins to luminesce; this is shown as the luminescence. The sampling pulse can then be delayed and upconverted with the PL to obtain time resolution of the PL intensity.

1.3 Previous Work

There have been several attempts to achieve TRPL at the Air Force Institute of Technology (AFIT) beginning in 1997 with Cooley. [7] Each experiment has added to the understanding of TRPL. Cooley began by investigating the Shockley-Read-Hall (SRH), radiative and Auger recombination rates of indium aluminium arsenide antimonide (InAlAsSb) multiple quantum well (MQW) diode laser structures emitting near 3.3 μm, and showed that the SRH rate dominated recombination at temperatures between 77K and 150K. Gorski [10] demonstrated the Auger rates were as low as reported by Cooley, and showed that increases in the InAs/GaInSb well width of a type-II MQW decreased the recombination time. Cumblidge and Johnson [8, 12] showed a curve fit of the PL data that forced one of the three terms in the rate equation to be non-physical.

This dissertation and these theses used a mode-locked titanium sapphire (Ti:Saph) laser operating at $\sim$ 800 nm. The linearly polarized light was rotated to 45° and split by a polarizing beam splitter into horizontally and vertically polarized light. The excitation of the semiconductor and the upconversion was provided by this 800-nm light. In the case when the cladding would have absorbed the Ti:Saph laser, the clad was removed to observe the carrier dynamics of the MQWs. The drawback of these studies was that the full device could not be studied. Roberts [20] introduced an optical parametric oscillator (OPO) to attempt to excite the core of type-II MQWs without removing the clad; however, he was only able to achieve time-averaged PL with a Spectra-Physics Opal OPO.

1.4 Approach

In an interband IR semiconductor, recombination after an impulse excitation does not occur instantaneously, rather it occurs over a period of nanoseconds [10]. To develop lasers capable of delivering additional power on target, the electrical properties of semiconductors need to be investigated. Studied semiconductors include intrin-

sic InAs, $AlAs_{0.085}Sb_{0.915}/In_{0.88}Al_{0.12}As_{0.878}Sb_{0.122}$ type-I MQW and $InAs/Ga_{0.85}In_{0.15}Sb$ type-II MQW. [8]

As stated in Section 1.3, previous work used a mode-locked Ti:Saph laser operating at 0.800 μm and removed the clad in the semiconductor opto-electronic structure. The procedure used in this thesis retains the clad and adds a synchronous OPO which allows 0.832-μm light from the Ti:Saph to be converted to 1.300-μm and 2.311-μm beams. The 2.311-μm beam is used to excite the core of the semiconductor structure and the 1.300-μm is used as the sampling pulse.

For this procedure to work, a technique to set up and align the equipment needs to be established. A thermal camera and an IR sensitive card will aid in the establishment of ZPL. Following an attempt at ZPL, PL was detected from a MWIR semiconductor.

1.5 Problem Statement

Since laser development is an exercise in efficiency, the study of carrier dynamics of potential semiconductors is an important step in determining effectiveness of a semiconductor laser. Observing the temporal decay of the PL of an excited sample will allow the temporal decay of the carrier densities to be determined. From these densities, the coefficients of the rate equation (A, B and C) can be fit.

Previous research investigated carrier dynamics with a higher photon energy Ti:Saph laser. This study will introduce an OPO to reduce the photon energy of the excitation pulse to better examine the QW carrier dynamics. It will also produce documentation and a procedure for the setup of upconversion to be used for future study of TRPL.

1.6 Results

This thesis provides a step-by-step process for aligning, using and calibrating a Ti:Saph laser and a synchronous OPO; establishing sampling, excitation and PL

pathlengths; collection of PL; selection of a nonlinear crystal for upconversion; and attempting to find ZPL for the collection of the upconverted signal for analysis.

1.7 Overview

This thesis is broken up into five chapters and one appendix. Chapter Two discusses the theory of carrier dynamics. Chapter Three describes the experiment. Chapter Four details the results and Chapter Five is the conclusion. The appendix includes a discussion of software and the Mathematica® code used in this thesis.

II. Theoretical Formulation

The lasing efficiency of a MWIR semiconductor structure is highly dependent on carrier dynamics. Besides radiative decay, there are also non-radiative effects that heat the material and reduce efficiency. A better IR laser, using a MWIR material, requires better characterization of these non-radiative effects. Understanding these effects allows semiconductor crystal growers to design better structures to mitigate the non-radiative transitions. This would lead to higher power IR lasers suitable for defense applications.

2.1 Background

2.1.1 Quantum Wells. MWIR structures are manufactured by epitaxial growth on a crystalline structure. There are three kinds of epitaxial structures for semiconductors: types-I, -II and -III MQWs. Type-I MQWs are characterized by having the QW in the conduction and valence bands completely contained in a single layer. Type-II MQWs are created when the QW in the conduction band is in one layer and the QW in the valence band is in the adjacent layer. Finally, a type-III MQW is created when the conduction band edge of one layer has a lower energy than the valence band edge of the adjacent layer. Carriers can still transition from the conduction band to valence band as the allowable conduction band energies are higher than the allowable valence band energies. Figures 2.1 (a)-(c) illustrate the energy gaps as a function of location in the structure.

2.1.2 Electron-Hole Pair Formation and Recombination. Photon absorption works by taking the energy from a photon to promote an electron over the band gap. This process is instantaneous. This absorption creates an electron-hole pair, which is generally excited deep into the bands. The electron and hole then relax through carrier cooling to the band edge. This process is on the order of picoseconds. Finally, the electron-hole pair relax in the form of recombination. This last process occurs over a period of nanoseconds.

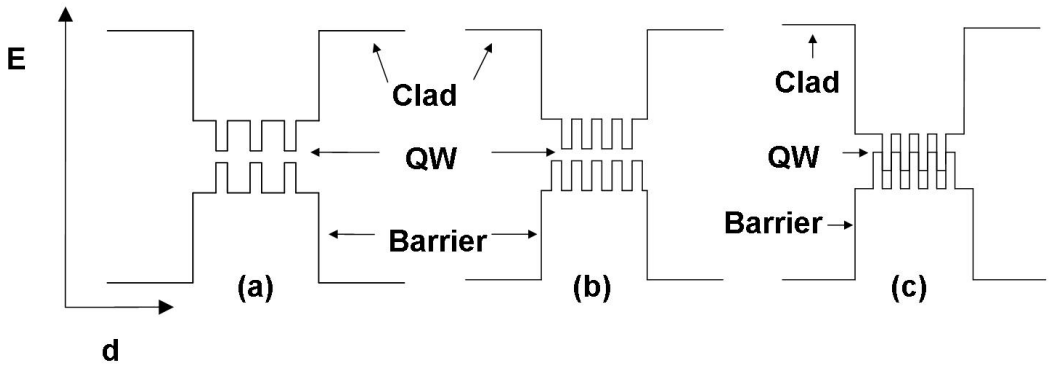

Figure 2.1. Energy diagram for types-I (a), -II (b) and -III (c) MQW. The outer, protective layer is known as the cladding.

Carrier recombination is characterized by three types of transitions: radiative, trap or defect, and Auger. Defect is one of the undesirable transitions. Figure 2.2(a) illustrates how an excited electron can decay from the conduction band to the valence band in several steps. Each step is caused by impurities in the semiconductor resulting in energy levels within the designed band gap. This releases several phonons instead of the desired single photon. Radiative recombination is the preferred transition as it releases a photon of approximately the band gap. When the sample is excited by optical radiation, this is PL. Figure 2.2(b) shows this recombination. Finally, Auger recombination is defined as a three-body transition. It involves an electron in the conduction band transitioning to the valence band. The energy from this transition is not released as a photon, but rather is used to excite a second electron from deep in the valence band to another valence band state. This second, now excited, electron is then free to return to thermal equilibrium without releasing a photon. This process is shown in Figure 2.2(c). This is the second undesirable form of recombination.

2.2 Theory of carrier dynamics

Once an electron-hole pair is generated, the system is no longer in thermal equilibrium. However, as in section 2.1.2, the intraband relaxation of the electrons and holes occurs over picoseconds; the conduction band electrons can be considered

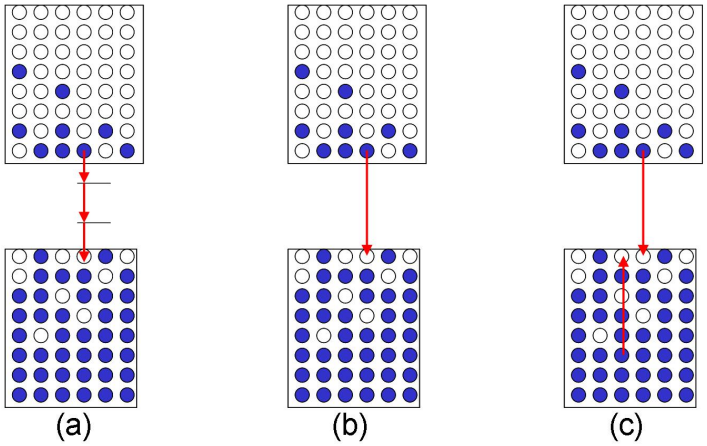

Figure 2.2. Illustration of the three forms of recombination: defect (a), radiative (b) and Auger (c). Radiative recombination is the preferred recombination.

in equilibrium among themselves, as are the valence band holes. This situation is known as quasi-equilibrium.

The development for calculating the carrier density begins with the density of states for the electrons and holes, which are defined as

$$\begin{aligned} \varrho_c(E) &= \frac{(2m_n^\star)^{3/2}}{2\pi^2\hbar^3}\sqrt{E-E_c}dE \\ \varrho_v(E) &= \frac{(2m_p^\star)^{3/2}}{2\pi^2\hbar^3}\sqrt{E_v-E}dE. \end{aligned} \tag{2.1}$$

where $\hbar$ is the Plank constant divided by 2π, $m_n^{\star 3/2}$ and $m_p^{\star 3/2}$ are the effective masses of the electrons and holes, respectively, E is the energy, and E_c and E_v are the band edge energies for the conduction and valence bands respectively. The first equation is the density of states for the electrons in the conduction band and the second is the density of states for the holes in the valence band. [15] Fermi-Dirac statistics provide the next step as the distribution, $f_n(E)$, represents the probability a conduction-band energy level, E, is occupied by an electron. $f_p(E)$ then represents the probability a valence-band energy level, E, is occupied by a hole. Equation (2.2) shows the

respective distribution functions.

$$f_n(E) = \frac{1}{1 + e^{(E_c - E_{fc})/kT}}$$
$$f_p(E) = 1 - \frac{1}{1 + e^{(E_{fv} - E_v)/kT}} \tag{2.2}$$

E_{fc} and E_{fv} are the quasi-Fermi levels for the conduction and valence bands, respectively.

The carrier densities are then $n(E) = \varrho_c(E) \cdot f_n(E)$ for electrons and $p(E) = \varrho_p(E) \cdot f_p(E)$ for holes. [15,24] Figure 2.3 illustrates a semiconductor in quasi-equilibrium. It shows the two distribution functions and the resulting carrier densities in each band.

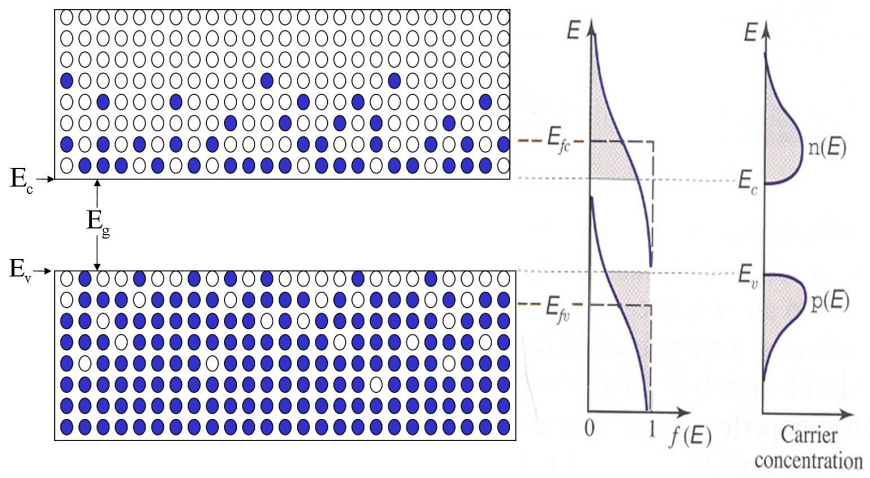

Figure 2.3. A semiconductor in quasi-equilibrium. $f_n(E)$ is the probability that a conduction-band energy level E is occupied by an electron. The probability that a valence-band energy is occupied by a hole is 1 - $f_p(E)$. n(E) and p(E) are obtained by multiplying the Fermi function by the density of states. [21]

2.2.1 Carrier densities from intensity. The rate equation now needs to be related to a measurable value. Since the PL signal can be measured and not the

carrier density directly, the rate equation needs to be related to the PL. From

$$n(t_0) = \frac{\epsilon}{h \cdot \nu}\left(\frac{2}{N_{qw} \cdot \pi \cdot w_{pl}^2 \cdot t_B}\right)(1-R)\cdot$$
$$(1 - exp[-\alpha \cdot N_{qw} \cdot (t_B + t_{BAR})])\left(\frac{1}{1+\frac{w_p^2}{w_{pl}^2}}\right) \tag{2.3}$$

the relation between PL intensity and carrier density can be established. [7] $n(t_0)$ is the initial, and maximum, carrier density in the QW at excitation. ϵ is the energy per pulse and is divided by the energy per photon, $h \cdot \nu$. N_{qw} is the number of QWs. w_p and w_{pl} are the waist of the pump and PL, respectively. R is the Fresnel reflection at the semiconductor surface. α is the absorption coefficient. Finally, t_B and t_{BAR} are the thicknesses of the QW and barrier, respectively, within the semiconductor structure. Equation (2.3) is used to calculate the initial carrier densities at various excitation powers and is plotted against the experimentally measured PL intensities at the same excitation powers. This curve is shown in Figure 2.4. [10]

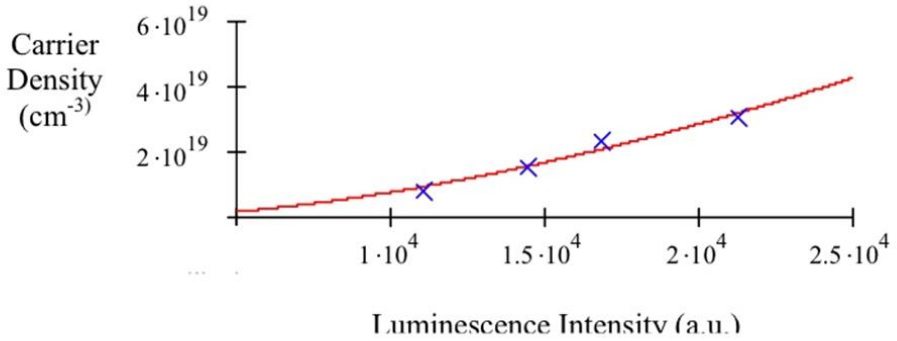

Figure 2.4. A plot of carrier density as a function of luminescence. [10]

The equation used to fit the data in Figure 2.4 is given by

$$n(L) = u_1 \cdot L + u_2 \cdot L^{u_3} \tag{2.4}$$

where u_1, u_2 and u_3 are coefficients that provide the best fit. Using TRPL, the carrier densities can then be plotted as a function of time.

2.3 Theory of Upconversion

TRPL is contingent on obtaining upconversion of the PL. Upconversion is the process of sum frequency generation (SFG). SFG occurs when two optical waves of different frequencies are mixed to generate a third wave of a higher frequency. This mixing occurs when the energy conservation and phase matching conditions are met. The energy conservation condition is

$$\omega_1 + \omega_2 = \omega_3. \tag{2.5}$$

where $\omega_{1,2}$ are the frequencies of the input beams and ω_3 is the frequency of the output beam. The phase matching condition is

$$\mathbf{k}_1 + \mathbf{k}_2 = \mathbf{k}_3 \tag{2.6}$$

where $\mathbf{k}_{1,2,3}$ are the propagation vectors of the input and output beams, respectively. The difficulty obtaining SFG comes from simultaneously solving Equation (2.5) and (2.6).

SFG will not occur in an isotropic material; it will only occur in anisotropic media. There are two kinds of anisotropic crystals: uniaxial and biaxial. Biaxial crystals have three different principle indices of refraction. Due to symmetry of the crystalline structure, uniaxial crystals only have two indices of refraction known as an ordinary index, n_o, and an extraordinary index, n_e. A positive uniaxial crystal has $n_e > n_o$; a negative uniaxial crystal has $n_e < n_o$. The different indices of refraction raise an additional challenge to phase matching as polarization also needs to be considered.

Using a negative uniaxial crystal as an example, the phase matching condition for the collinear case becomes

$$n_e(\omega_1) \cdot \omega_1 + n_o(\omega_2) \cdot \omega_2 = n_e(\omega_3) \cdot \omega_3 \tag{2.7}$$

An example of a negative uniaxial crystal is lithium iodate ($LiIO_3$). This crystal is important because it allows phase matching for ZPL. As Figure 1.2 showed, $\mathbf{k}_1$ and $\mathbf{k}_2$ are not collinear. This results in n_e being a function of incident angle, as well as ω. However, the complications of SFG are simplified by the use of two software programs: SNLO nonlinear optics code and a Mathematica notebook. Using these two programs, the numerical challenges are alleviated. Additional discussion of these programs is included in Appendix A.

2.4 Summary

Carrier dynamics and SFG were discussed in this chapter. TRPL uses SFG to provide time resolution of PL decay. Relating the carrier densities to the intensity of the PL provides time resolved carrier dynamics. The resultant data can then be fit to the rate equation to obtain the recombination coefficients.

III. Experiment

This chapter discusses the experimental setup, equipment used, and the documented procedure for TRPL.

3.1 Experimental Procedure

TRPL spectroscopy was first described by Mahr [14] and detailed by Shah. [22] It allows for the characterization of PL on a time scale of the same order as the excitation pulse. The intensity of the upconverted PL pulse is related to the carrier densities via the relationships as discussed in Chapter 2. These carrier densities are then used to fit theoretical models describing radiative and non-radiative relaxation processes.

3.2 Experimental Setup

This thesis uses a mode-locked Ti:Saph laser and a synchronous OPO to generate the photons of proper wavelength necessary to excite the core of various MWIR semiconductor structures. There are four distinct optical paths: sampling (signal beam), excitation (idler beam), luminescence (PL), and upconverted. Figure 3.1 shows the setup of this experiment. The sampling path has a fixed optical path length (OPL) and has a focus at the non-linear crystal. The second path, the excitation path, travels a variable OPL and is incident on a liquid nitrogen cooled semiconductor. The variation of this path is provided by a translatable mirror which is able to temporally shift the luminescence relative to the arrival of the sampling pulse. By shifting the start of PL, the sampling path is able to experience upconversion with the luminescence path - the path from the semiconductor - at the non-linear crystal at various times along the PL lifetime. The fourth path is the upconverted signal as it exits the non-linear crystal and is directed to a photomultiplier tube (PMT).

3.2.1 Pump laser. The first component of this setup is a Coherent Verdi Nd:YVO_4 laser operating at a wavelength of 532 nm. The operating power is 12.5

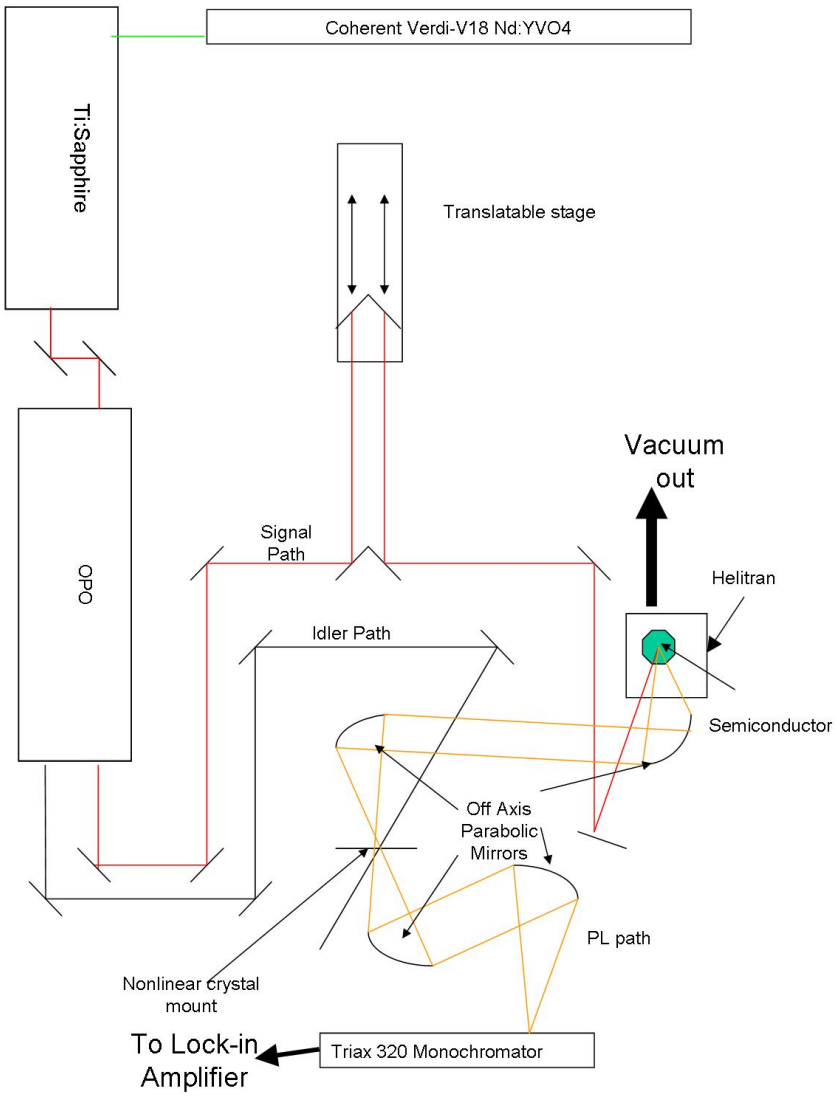

Figure 3.1. Setup of the TRPL equipment

W. It uses a water cooler as a heat sink. To prevent damage to the laser, the cooler needs to be at 18°C; cooling can take up to 15 minutes to reach steady state.

3.2.2 Ti:Saph laser. [6] The Verdi enters a Coherent Mira Ti:Saph femtosecond laser. This laser amplifies wavelengths between 680 and 1100 nm and further restricts the wavelengths to 150-nm ranges centered on three wavelengths. Each lasing wavelength requires that the cavity be an integer number of wavelengths; this is known as a longitudinal mode. It utilizes mode-locking to create a pulsed laser operating at 76 MHz at 1.4 W. Mode locking occurs when the frequencies generated undergo destructive interference from all available modes excepting at the pulse where the modes constructively interfere. More modes available yield a smaller pulse width so a high modal volume is encouraged. The Ti:Saph crystal absorbs the 500-nm light from the pump and reemits is at the available frequencies.

This study requires the OPO to receive light of 832 nm. Since there is a water absorption line at 820 nm, the humidity is monitored and controlled. There is a relative humidity monitor included on the controller for the Ti:Saph which should be below 25% for mode locking to occur. If the humidity is above 25%, then the humidity can be controlled via a nitrogen tank connected to the Ti:Saph.

For ease of use of the OPO, maximum power is required. After turning on the Verdi, there is a start-up period of about 2 minutes as the power slowly ramps up to the operating condition. After this start up period, the power for a given wavelength should be maximized. This is accomplished by tuning the pump optic mirrors, the flat end mirror and the slits, all as described in the manual.

By adjusting the birefringent filter, the wavelength can be adjusted between 680 and 1100 nm. Rotation of the control clockwise decreases the wavelength while a counterclockwise rotation increases it. As the wavelength is adjusted in small increments, the laser should be kept mode locked and at maximum power. The wavelengths that are only achievable as a continuous wave should be avoided for use in the OPO.

3.2.3 OPO. [3] The 830-nm mode-locked Ti:Saph laser enters the Coherent OPO from a pair of mirrors as depicted in Figure 3.1. Upon entering the device, the light enters a ring mirror configuration. Within the OPL of the PP830-Ring cavity, there is a nonlinear crystal. When under a stress, it downconverts the incoming Ti:Saph laser into two parts. The idler and signal do not exit the OPO at the same time; the signal leads the idler by 3 ns. This will be discussed further in the alignment procedure.

3.2.3.1 Discussion. The downconversion of the Ti:Saph is an important process to understand, as the idler is key to PL. Upconversion and downconversion require the conservations of energy and momentum. Since the pump Ti:Saph is lasing at 832 nm and the OPO signal will nominally be set to 1300 nm, from Equation (3.1), the idler will be at 2311 nm. Since the idler will be incident on the semiconductor, the photon energy needs to be such that the core of the MWIR device structure will be excited while the clad remains transparent to this energy.

$$\frac{1}{\lambda_{Ti:Saph}} = \frac{1}{\lambda_{Idler}} + \frac{1}{\lambda_{Signal}} \tag{3.1}$$

3.2.3.2 Operation. The OPO outputs three lasers: a tunable signal, a feedback signal, and an idler. To begin, the feedback signal must be sent into a spectrometer; however, directing the full intensity of the laser into the spectrometer will irreparably damage it. Instead, a beam splitter must be used to reduce the irradiance. Also, due to the path in the OPO, there are three beams exiting; the strongest of the three is to be directed into the spectrometer. This feedback provides the OPO software a response to the adjustments to the OPO controller. The pump and signal will be detected and displayed on the control screen when the path is aligned. Alignment is done by directing the strongest beam into the center of the focusing lens and then into the entrance slit. If the beam does not enter the center of the focusing lens and entrance slit, there will be no signal displayed.

Since tuning for the bulk crystal is conducted via pump wavelength tuning, prior knowledge of the Ti:Saph laser wavelength is needed or guess work will be necessary. The piezo voltage applied to the non-linear crystal can be modulated between 0 and 4095 in arbitrary units. Based on the incoming wavelength, the voltage needs to be approximately tuned based on Table 3.1. In addition to changing the piezo voltage, for λ_{Signal} between 1100 and 1200 nm, the 6-mm dispersion block should be used. For all λ_{Signal} greater than 1200 nm, the 12-mm dispersion block is required. Below λ_{Signal} of 1100 nm, no dispersion block should be used.

Table 3.1. Variation of pump wavelength to OPO output based on Mira documentation

λ_{Signal} (nm)	Power (mW)	$\lambda_{Ti:SAFF}$ (nm)	Piezo Voltage (A.U.)
1100	500	840	148
1150	560	829	500
1200	500	829	1100
1250	450	829	
1300	400	830	1700
1350	380	832	1748
1400	250	831.5	
1450	240	831.5	2148
1500	320	831.5	
1550	280	831.5	
1600	150	836	2678

Variation in day-to-day operation of the equipment requires a daily tuning of the piezo voltage to yield the desired output signal wavelength. The controller can automatically control the signal within a user-specified tolerance (up to $\Delta\lambda = 1nm$) provided the signal from the feedback is strong enough to be detected. If the feedback wavelength is weak, the input from the Ti:Saph needs to be adjusted as detailed above.

The controller is an APE OPO PP Automatic supplied from Coherent with the OPO. The different display options are shown under "Spectrum Menu". From here, the pump, signal, and a "vis" wavelength can be displayed. Specific to this thesis, the "vis" was not seen and was not needed. [3]

The signal can be tuned from 1100 - 1600 nm based on the input pump wavelength and piezo voltage. Setting the signal is done by slowly adjusting the pump wavelength while keeping a mode-locked laser until the desired pump wavelength is reached. Once the Ti:Saph is set to the proper wavelength, Table 3.1 gives a range for the piezo voltage. Caution is advised when operating on a pump wavelength that is barely detectable, as fluctuations in operating conditions can reduce the signal below the detection threshold. This causes the automatic piezo control to attempt to find the signal again by increasing the piezo voltage. This can ruin a data run if the signal is not optimized. The signal is used as the sampling light.

The OPO that is used has had the idler option installed. The idler is the excess from the downconversion process, and while not directly monitored, is related to the input and signal wavelengths via Equation (3.1). The idler is used to excite the semiconductor structure's inner active region. The idler beam also has components from the pump at 832 nm in addition to the 2311-nm light. The 832-nm component was reduced by placing a long pass filter in the path of the idler.

3.2.4 Alignment. Alignment for this procedure is crucial to success. The OPLs for the three paths are on the order of meters. As a result, if the laser is not centered on the center of the mirrors, alignment becomes challenging.

3.2.4.1 Zero path length. Since the signal and the idler have different OPLs inside the OPO, they exit at different times. Since the upconversion process will require phase matching, the OPLs on the optical table must be established such that the overall OPL of each path is the same. The idler leads the signal by 10 ns or the signal leads the next idler pulse by about 3 ns. Based on the configuration of the table, the idler path is 5.35 m at a minimum; the signal path is 2.53 m at a minimum. The signal path needs to be either 0.9 m longer than the idler path or 2.998 m shorter. Since the signal path is 2.82 m shorter, the idler path can be increased by 0.178 m to get ZPL. Fine adjustments in the OPL is accomplished with the translatable stage.

Previous work used an IR sensitive card from Spectra-Physics or night vision goggles to directly observe the Ti:Saph laser. Since both the signal and idler have a longer wavelength, neither technique worked well for this research. The solution to this problem was to use an Inframetrics 760 thermal viewer and a Thorlabs VC-VIS/IR card. The IR viewer requires approximately a 10 minute startup time to allow the camera to cool down. To use the thermal camera, the idler was allowed to heat a piece of cardstock to a temperature detectable by the IR viewer. The challenge of this technique is that the response time is approximately 20-30 seconds of heating/cooling to detect variations in the alignment. This technique worked well when the mirrors were across the table from each other. When the mirrors were on the same side of the table, the VC-VIS/IR card with the night vision goggles was able to detect the signal only in a darkened room. The VC-VIS/IR card can detect the signal component directly. The difficulty with this method of detection is that if the power from the OPO is not maximized, by having the power from the Ti:Saph maximized, then the intensity reradiating from the IR card will be weak.

For ZPL, the laser pulses must be phase matched at the $LiIO_3$ crystal. In addition, they need to be overlapping. By replacing the $LiIO_3$ crystal with a pinhole, it can be assured the beams occupy the same space by passing the idler and the signal beams through the pinhole. A photodetector is employed for alignment on the other side of the pinhole. By adjusting the focusing mirror directly preceding the pinhole, and passing the lasers through, the intensity in the photodetector can be maximized. This corresponds to a focus at the pinhole. At this point, the paths are aligned up to the non-linear crystal.

To align the PL path, a Helium Neon (HeNe) laser was placed in line with the Triax 320 monochromator as in Figure 3.1. It was projected between the off-axis parabolic mirrors towards the pinhole. Next, it was focused through a 63-mm lens, through the pinhole, where the signal was maximized with the photodiode. It was then projected between the other pair of off-axis parabolic mirrors onto the cold finger in the vacuum chamber.

3.2.5 Procedures. The following section describes the methodology to turn on the equipment used, adjust it and shut it down.

3.2.5.1 Startup of the Lasers.

1. Turn on chiller to the Verdi Nd:YVO_4. Allow it to reach 18°C.
2. Once the chiller is at 18°C, turn on the Verdi and open the aperture.
3. Allow a 2 minute warmup time.
4. The Ti:Saph should be adjusted for maximum power and mode-locked. If mode-locking is not possible, reduce the humidity to below 25%.
5. Turn on the OPO controller.
6. Adjust the piezo voltage to 1700 and look for a signal.
7. Adjust the piezo voltage to get the signal to 1.300 μm.
8. Adjust the Ti:Saph to maximize the power in the signal.
9. If there is no signal, go to the pump display screen and make sure the Ti:Saph is set to 832 nm. Repeat 6-8.

3.2.5.2 Startup of the PL Equipment.

1. Get liquid nitrogen (LN2) from the cryo-room.
2. Cool the monochromator and the cold finger with LN2.
3. Turn on SRS540 chopper wheel, SR850 lock-in amplifier, Jobin Yvon DataScan2, IG4400 Ionization Gauge Controller, Alcatel CFV vacuum system and Lakeshore 330 Autotuning Temperature Controller.
4. Start the SynerJY software.
5. Initalize the software to collect PL.
6. Start collecting PL.

3.2.5.3 Alignment. The first time the system is aligned.

1. Turn on the Inframetrics IR viewer and allow to initialize. Ensure the cap is on the lens.
2. Starting with either the signal or idler path, use the night vision goggles and IR card to see where the beam is.
3. Adjust each mirror's tip and tilt to steer the beam to the next mirror.
4. When the beam is too faint to see with the night vision goggles due to divergence, place a beam block in the path.
5. Allow the beam block to heat up and observe with the IR viewer.
6. Make small changes to the previous mirror's tip and tilt and wait to see the thermal changes.
7. Repeat 6 until the beam is centered on the next mirror.
8. Continue using the IR viewer and beam block to align the remaining mirrors.
9. Repeat steps 3-8 with the other path.

3.2.5.4 Daily alignment.

1. Place the pinhole in the crystal mount.
2. Use the photodiode to measure the irradiance of the idler and PL.
3. Adjust the focusing mirror (for the PL) or lens (for the idler) to maximize signal.

3.2.5.5 Shutdown.

1. Shutdown is the reverse of startup.

3.3 Description of the sample

This experiment will use a p-doped InAsSb epitaxially grown bulk semiconductor as the sample. It was chosen for its large surface area, as this allows the most

leniency in alignment. The structure of the sample is shown in Figure 3.2. The 41-period superlattice is used for lattice matching from the p-55%AlGaAsSb and the p-InAsSb. The first period has a layer of 123 Å for the AlGaAsSb and 3 Å for the InAsSb. For each period, the AlGaAsSb thickness decreases by 3 Å and the InAsSb thickness increases by 3 Å. These periods result in a final layer of 3 Å of AlGaAsSb and 123 Å of InAsSb.

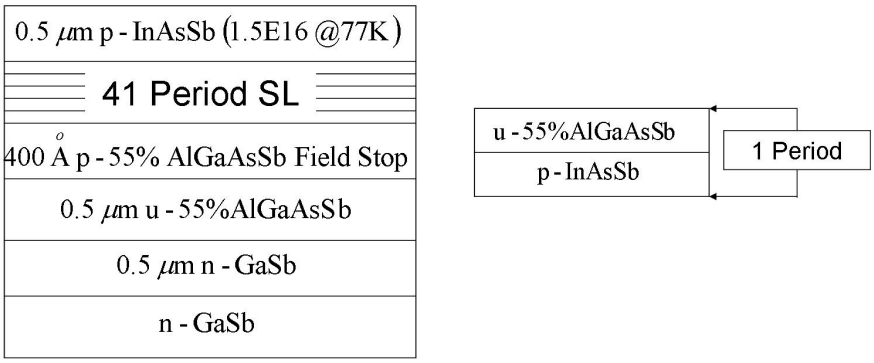

Figure 3.2. An illustration of the structure of p-InAsSb sample

3.4 Summary

This section contains a detailed look at the equipment used in TRPL. It also includes an enumerated list of procedures for starting up the lasers, starting the equipment, aligning the optics and shutting down the system.

IV. Results

There were two additional goals beyond supplying documentation for the setup of TRPL and operating procedures. These goals where to find ZPL and observe PL from a sample semiconductor. Since the signal and idler beams were low power and difficult to align, ZPL was challenging to find. In addition, collecting PL and directing it to the monochromator proved difficult with the low intensity PL. ZPL was attempted with a $LiIO_3$ crystal cut at 20.3°, and the idler and signal beams at ordinary polarizations to the crystal.

4.1 ZPL

One goal of this experiment was to obtain ZPL. This was not obtainable because the upconversion efficiency kept the power of the upconverted beam below detection with the photodiode. To obtain ZPL, a PMT would need to be used. Trying to obtain ZPL with the signal and idler from the OPO consumed vast quantities of time. One idea to improve the efficiency is to try to find a nonlinear crystal with a higher d_{eff} as the SFG efficiency is proportional to d^2_{eff}. [23] This would require close examination of each nonlinear crystal possible and would be time intensive.

4.2 PL

A second goal of this thesis was to obtain PL spectrums from a sample semiconductor. InAsSb was selected and its PL profile is shown in Figure 4.1. The peak intensity was shown to be at 3.8 μm (at $\sim$ 150K) for this sample of InAsSb. Roberts found the peak to be at 3.28 μm (at 80K) as shown in Figure 4.2. For TRPL, mixing for either of these wavelengths and the 1.300 μm signal beam can still be accomplished with a $LiIO_3$ crystal.

4.3 Varshni Equation

To compare the PL values of 3.28 and 3.8 μm at two different temperatures needs to take the Varshni equation into consideration. The Varshni equation relates

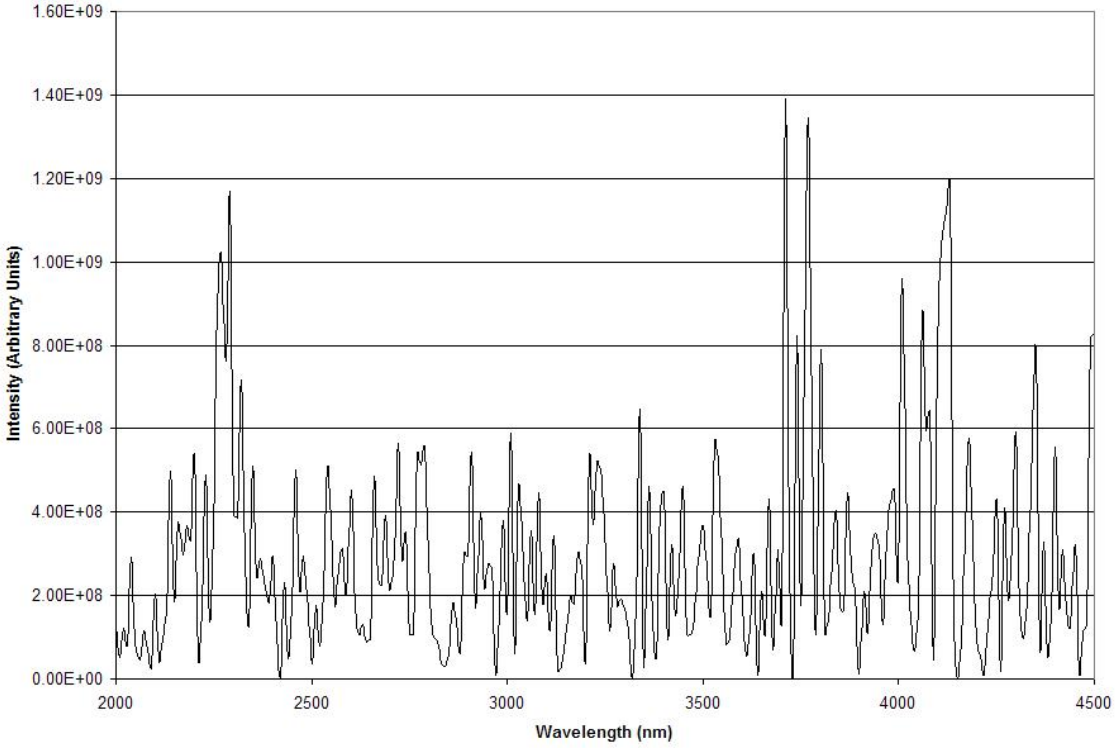

Figure 4.1. PL for InAsSb from 2000 to 4500 nm. T = 150K

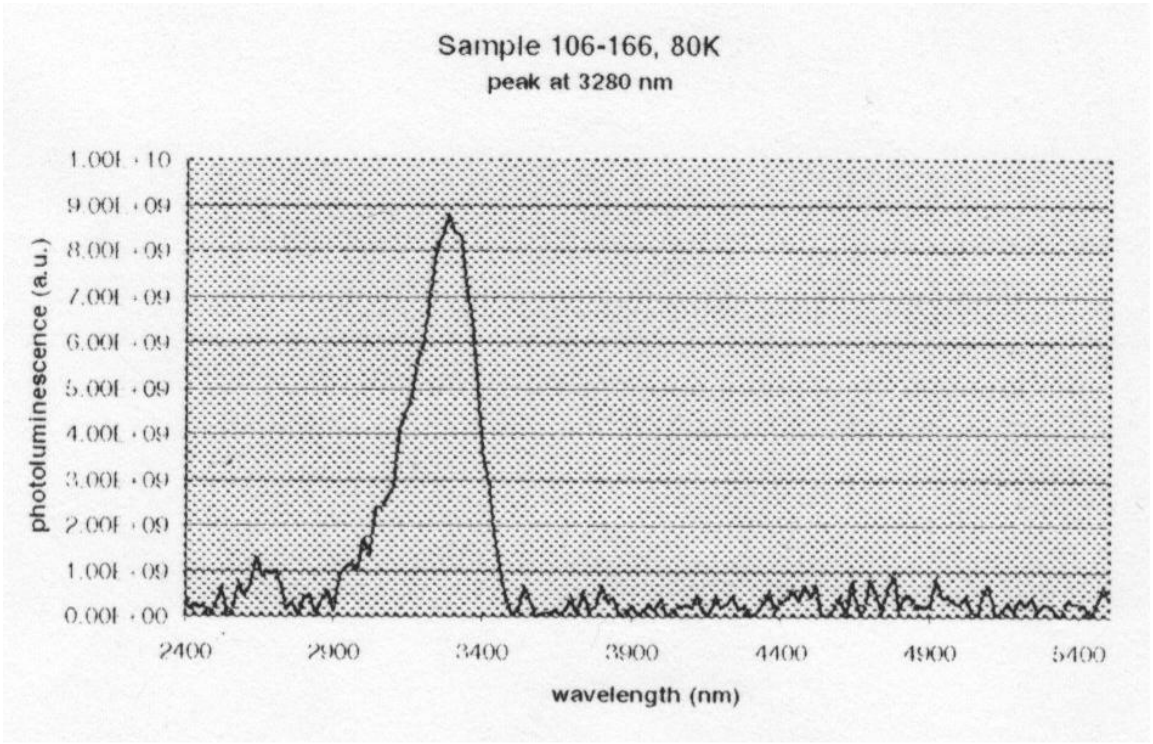

Figure 4.2. PL for InAsSb from 2400 to 5500 nm from Roberts. T = 80K

the band gap energy to temperature, and is defined as

$$E_g(T) = E_g(0K) - \frac{\alpha T^2}{\beta + T}, \tag{4.1}$$

where E_g is the energy of the band gap, T is the temperature and α and β are constants determined by the material. For InAs, $E_g(0K)$ is 0.415 eV, α is $2.76 * 10^{-4}$ $\frac{\text{eV}}{\text{K}}$ and β is 83K. This gives units of eV to $E_g(T)$. The corresponding wavelength is then

$$\lambda = \frac{h \cdot c}{E_g(T)}. \tag{4.2}$$

For T = 80K, λ = 3.07 μm. For T = 150K, λ = 3.19 μm. However, the addition of Sb would shift the energies. Taking 3.28 μm as the correct value for 80K, this gives a $E_g(80K)$ of 0.404 eV. This is a shift of -0.026 eV from the value for InAs. Applying the same shift to $E_g(150)$ yields 0.324 eV. This energy corresponds to a PL wavelength of 3.83 μm.

4.4 Summary

PL from an InAsSb MWIR sample at 150K was found to be located at 3.8 μm. This is in agreement with Roberts measurement at 80K. ZPL was not found due to the time required to align the optics.

V. Conclusions

The objective of this research was to improve on the technique for TRPL. This chapter summarizes the efforts and recommends future work.

5.1 Summary

TRPL with the signal and idler outputs from an OPO is a difficult and time consuming technique to measure carrier dynamics of semiconductors. Without a well documented methodology, this work becomes almost impossible to accomplish in a timely fashion. Documentation and techniques used during previous efforts have been changed by the introduction of an OPO. In addition, upconversion was attempted with the 1.300-μm signal and 2.311-μm idler beams of the OPO with a $LiIO_3$ crystal cut at 20.45° oriented at +0.33°.

PL data was collected for a sample InAsSb semiconductor showing the peak luminescence was at 3.8 μm. This wavelength can be mixed with the sampling beam within the $LiIO_3$.

5.2 General Recommendations

Future work would be to continue the efforts at improving the methodology of TRPL or to use the available documentation to investigate the carrier dynamics of various semiconductors. This effort focused on the procedures for the setup of TRPL whereas the continued improvements would be centered on the collection and analysis of data from the luminescence.

As stated in Chapter 2, the use of SRH, radiative and Auger coefficients can be improved on by expanding the rate equation and keeping the higher order terms for MQW semiconductors. For bulk semiconductors, the use of the SRH, radiative and Auger coefficients is sufficient for realistic values.

Appendix A. Software

This appendix describes the selection of crystals for use in upconversion. There are two steps involved in selection: use of SNLO and Mathematica®.

A.1 SNLO

SNLO nonlinear optics code is a Windows®-based program to assist in selecting a nonlinear crystal among other features. One feature of SNLO is the ability to choose incident wavelengths and available non linear crystals. It also computes phase matching angles based on polarization and the angle of the crystal face to the incident beams.

SNLO is made available by A.V Smith at Sandia National Laboratories (SNL). It is no longer maintained by SNL but can still be downloaded from the internet. [2]

Table A.1 shows a sample of the SNLO output for the "Qmix" module using input parameters of a $LiIO_3$ crystal and 1.300-μm and 2.311-μm wavelengths.

Table A.1. Sample Output Table from SNLO

2311.0 (o) + 1300.0 (o) = 832.0 (e)				
Walkoff [mrad]	=	0.00	0.00	54.98
Phase Velocities c/	=	1.838	1.852	1.847
Group Velocities c/	=	1.868	1.875	1.889
GrpDelDisp (fs^2/mm)	=	-46.5	92.0	179.0
At Theta	=	20.3	deg	
deff	=	1.61E0	pm/V	
Field gain coeff.	=	6.39E-5	/sqrt.Watt	
Crystal ang. tol.	=	0.82	mrad·cm	
Temperature range	=	264.25	K·cm	
Mix accpt ang	=	2.29	1.28	mrad·cm
Mix accpt bw	=	48.15	74.16	cm-1·cm

A.2 Mathematica

Once the crystal had been selected via SNLO, it has to be placed at an orientation that could yield upconversion. The use of a numerical software package is

necessary to determine the orientation of the crystal. A Mathematica® notebook was prepared in a previous dissertation prospectus by LtCol Roberts [20].

The calculations below describe the use of this LiIO3 for an upconversion experiment, where a pulsed beam at 1300 nm wavelength (the "NL pump" beam) is used to time-resolve mid-IR (2-5 μm) photoluminescence from a semiconductor. The semiconductor is pumped by a pulsed 1300 nm beam (the "sample pump" beam) that has the same temporal characteristics (PRF and PW) as the NL pump beam.

Initialization

First, define alternate trig functions that use degrees instead of radians.

```
dSin[x_]:=Sin[Pi x/180]
dCos[x_]:=Cos[Pi x/180]
dTan[x_]:=Tan[Pi x/180]
dArcSin[x_]:=180ArcSin[x]/Pi
dArcCos[x_]:=180ArcCos[x]/Pi
dArcTan[x_]:=180ArcTan[x]/Pi
ϵ = 0.00000000001;
```

The index ellipsoid for LiIO3 (from Kato, same as used by SNLO) is:

```
ny[λ_]:=Sqrt[3.415716 + (0.047031/(λ^2 − 0.035306)) − 0.008801λ^2];
nz[λ_]:=Sqrt[2.918692 + (0.035145/(λ^2 − 0.028224)) − 0.003641λ^2];
```

The transmission window for LiIO3 is:

```
λ1min = 0.300;
λ1max = 6.000;
```

Sum Frequency Generation

The wavelengths we'll look at are (in μm):

(*λ1isthewavelengthtobeupconverted(PL, idler, orsignal)*)

λ2 = 1.300; (* the NL pump wavelength *)

λ3[λ1_]:=1/((1/λ1) + (1/λ2))(* the upconverted wavelength *)

Each of the three beams sees a different optical index:

n1[λ1_]:=ny[λ1]; (*ordinarybeam, y − polarized*)

n2 = ny[λ2]; (*ordinarybeam, y − polarized*)

n3[λ1_, θ_]:=ny[λ3[λ1]]nz[λ3[λ1]]/Sqrt[(nz[λ3[λ1]]dCos[θ])^2 + (ny[λ3[λ1]]dSin[θ])^2];

(*extraordinarybeam, xz − polarized*)

where θ is the angle from the z axis to beam 3.

Next, set up the phase matching requirement:

k1[λ1_]:=2Pin1[λ1]/λ1;

k2 = 2Pin2/λ2;

k3min[λ1_]:=Abs[k1[λ1] − k2]

k3max[λ1_]:=k1[λ1] + k2

k3[λ1_, θ_]:=2Pin3[λ1, θ]/λ3[λ1]

For example, consider upconversion of the 2311 nm excitation beam, scattered off the sample (for ZPL):

k1[2.311]

k2

k3min[2.311]

k3max[2.311]

Plot[{k3min[2.311], k3max[2.311], k3[2.311, θ]}, {θ, 0, 180}, AxesLabel → {"θ", "k"}];

4.99669

8.95029

3.9536

13.947

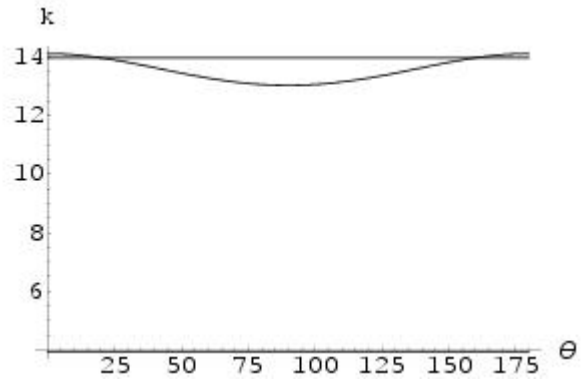

k3 needs to be between k3min = |k1-k2| and k3max = k1+k2 for phase matching to be possible. From the plot above, we see that this is only true over a limited range of θ:

θmin[λ1_]:=Replace[x, FindRoot[k3[λ1, x]==k3max[λ1], {x, 45}]]

θmax[λ1_]:=Replace[x, FindRoot[k3[λ1, x] == k3max[λ1], {x, 135}]]

Plot[k3max[x] − k3[x, 90], {x, 0.2, 10}, AxesLabel → {"θ", "k3max-k3"}];

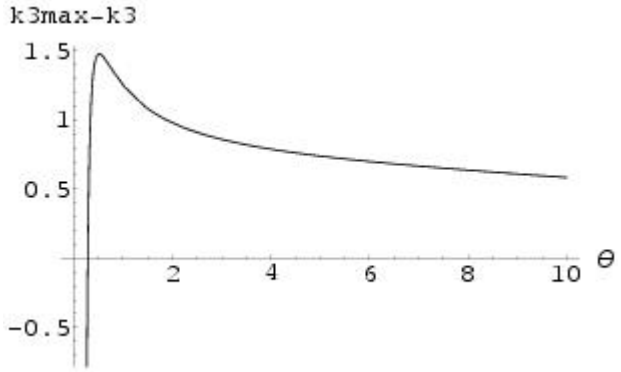

The above plot shows the range of PL wavelengths for which phase-matching can be achieved, assuming all input beams can be coupled into the crystal and that the crystal will transmit at the wavelengths involved. Where the function plotted is positive, phase-matching is possible. The lower limit is:

Replace[x, FindRoot[k3max[x] − k3[x, 90] == 0, {x, 0.4}]]

0.285172

which is outside the transmission window defined above, so the lower λmin needs to be reset to the initial valueis new value. The upper limit is obviously outside the transmission window, and so is unchanged.

Plot[{θmax[λ1], θmin[λ1]}, {λ1, λ1min, λ1max}, AxesLabel → {"λ1", "θ"}];

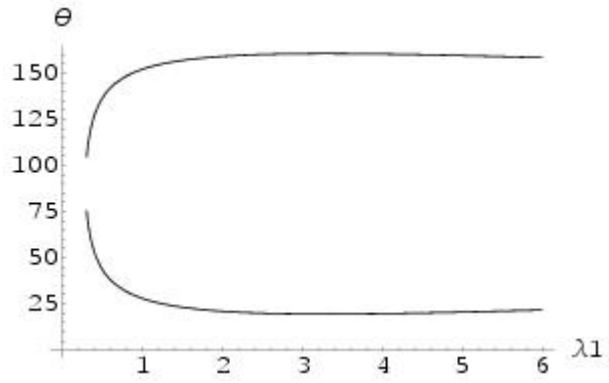

Continuing the ZPL example:

θmin[2.311]

θmax[2.311]

20.2703

159.73

Note that θmin and θmax correspond to the angles where k3 is exactly equal to k1+k2. This is the collinear case, and our θmin is within rounding of SNLO's prediction of a 20.3 degree phase-matching angle for photoluminescence at 2311 nm. As θ increases from θmin, k3 becomes less than k1+k2, so the angle between the k1 and k2 beams has to open up.

Now to calculate the angles α and β from the first beam to the second and third beams, respectively, using the law of cosines.

α[λ1_, θ_]:=dArcCos[(−k1[λ1]^2 − k2^2 + k3[λ1, θ]^2)/(2k1[λ1]k2)]

β[λ1_, θ_]:=dArcCos[(k1[λ1]^2 − k2^2 + k3[λ1, θ]^2)/(2k1[λ1]k3[λ1, θ])]

Plot[α[2.311, θ], {θ, θmin[2.311], θmax[2.311]}, AxesLabel → {"θ", "α"}];

Plot[β[2.311, θ], {θ, θmin[2.311], θmax[2.311]}, AxesLabel → {"θ", "β"}];

β[2.311, 90];

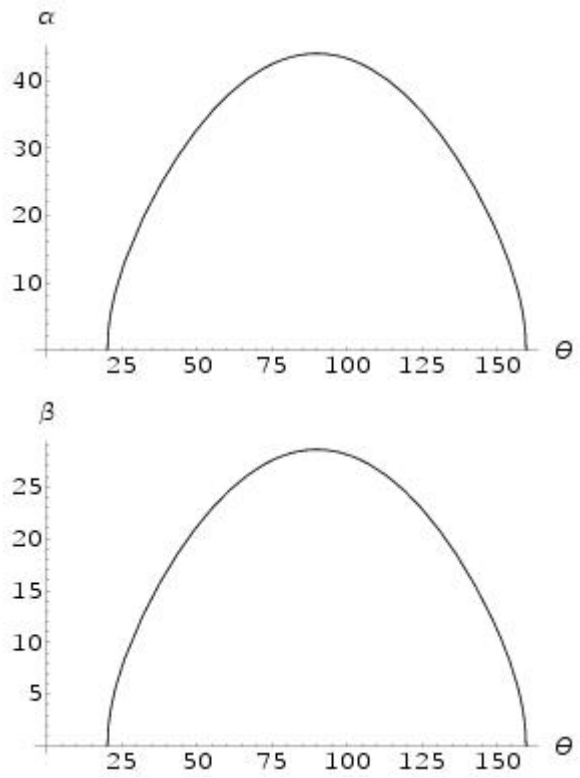

As expected, having $\theta = \theta$min corresponds to the collinear scenario, where α=β=0. It is also interesting to note that the maximum spread between the input beams (inside the crystal) that will still allow phase-matching is about 28.5 degrees.

All of the above angles are internal to the crystal. The angles outside the crystal need to be investigated, since that's what can be directly measured. For each value of θ, there is one and only one pair (α,β). Using Snell's law:

γ1[λ1_, θ_, ψ_]:=dArcSin[n1[λ1]dSin[$\theta - \psi + \beta$[λ1, θ]]]

γ2[λ1_, θ_, ψ_]:=dArcSin[n2dSin[$\theta - \psi + \beta$[λ1, θ] − α[λ1, θ]]]

γ3[λ1_, θ_, ψ_]:=dArcSin[n3[λ1, θ]dSin[$\theta - \psi$]]

The above equations have a new variable ψ to represent the cut angle of the crystal. It is the angle from the z axis of the crystal to the normal to its surface. Since

there are limits on θ, there may be limits on ψ also. In particular, all the external angles need to be in [-90,90] so that they will couple into/out of the crystal.

The upper limit on ψ is the lowest value that makes either $\gamma 1$ or $\gamma 2$ go to -90 degrees; the lower limit makes $\gamma 2$ or $\gamma 1$ go to 90 degrees. The limits on ψ are:

$\psi\text{min}[\lambda 1\_, \theta\_] := \theta + \beta[\lambda 1, \theta] - \text{dArcSin}[1/\text{n1}[\lambda 1]]$

$\psi\text{max}[\lambda 1\_, \theta\_] := \theta - \alpha[\lambda 1, \theta] + \beta[\lambda 1, \theta] + \text{dArcSin}[1/\text{n2}]$

$\text{Plot}[\{\psi\text{min}[2.311, \theta], \psi\text{max}[2.311, \theta]\}, \{\theta, \theta\text{min}[2.311], \theta\text{max}[2.311]\}, \text{AxesLabel} \rightarrow \{\text{"}\theta\text{"}, \text{"}\psi\text{"}\}];$

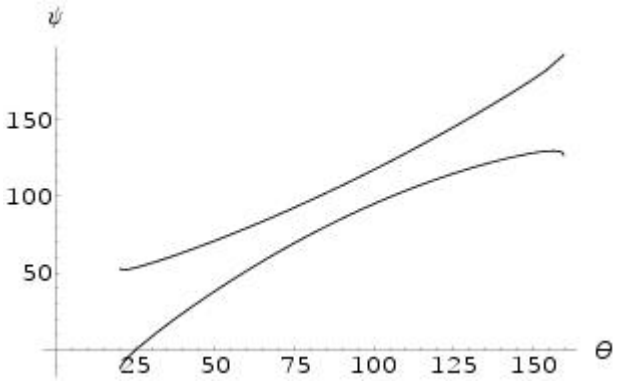

The above graph can be interpreted as follows. A horizontal line from the crystal cut angle on the vertical axis will intersect the two curves at the minimum and maximum values of θ for which all beams can be coupled into and out of the crystal, and that allow phase-matching for some (still undetermined) angle between the input beams. Alternately, for a given desired phase-matching angle on the horizontal axis, a vertical line can be drawn that will intersect the two curves at the minimum and maximum values of the crystal cut angle that will allow that particular configuration to be achieved. Yet another interpretation: All beams can be coupled into and out of the crystal, and phase-matching achieved, for any point (θ,ψ) inside the area bounded by the two curves and two vertical lines at θmin and θmax.

Now to calculate the orientations of the beams outside the crystal. In addition to the γ's defined above, δ is defined as the spread between the input beams for the positive and negative solutions.

$\delta[\lambda 1\_, \theta\_, \psi\_] := \gamma 1[\lambda 1, \theta, \psi] - \gamma 2[\lambda 1, \theta, \psi]$

Using the above equation, it is now possible to find the crystal orientation required to achieve phase-matching for a given wavelength input beam spread, δ, and crystal cut angle, ψ, by forcing the δ to match the experimental setup for all input parameters except θ, and then solving for θ. The solution can then be used to find $\gamma 2$, which is the angle between the normal to the crystal surface and the direction of the incoming NL pump beam. Since the direction and wavelength of the NL pump beam are fixed, it makes a good reference point for the orientation of the crystal. First it is necessary to "extend" the above definition of δ so that the function will produce an output (and not an error) for input values where δ is not defined (i.e. where phase-matching is not possible). Since δ will always be positive, extend the above definitions by making δ=-1 when it would otherwise not be defined, to eliminate ambiguity:

$$\boldsymbol{\delta e[\lambda 1\_, \theta\_, \psi\_]:=If[(\psi > \psi min[\lambda 1, \theta])\&\&(\psi < \psi max[\lambda 1, \theta]), \delta[\lambda 1, \theta, \psi], -1]}$$

For SHG of the NL pump beam, the interaction is collinear, so θ has already been calculated: it's θmin:

$$\boldsymbol{\theta min[2.311]}$$

$$\boldsymbol{Re[\psi min[2.311, \theta min[2.311]]]}$$

$$\boldsymbol{Re[\psi max[2.311, \theta min[2.311]]]}$$

20.2703

-12.6945

52.9544

Again, the phase-matching angle agrees with SNLO's prediction of 20.3 degrees. Since our crystal cut angle of 20.45 degrees is in the range (-12.7, 52.95), phase-matching will be possible and will happen at the crystal orientation:

$$\boldsymbol{Re[\gamma 2[0.775, \theta min[2.311], 20.45]]}$$

-0.315256

The crystal mount will not block the beam at this angle.

For ZPL, the spread angle becomes 22.4 degrees and the input wavelength is that of the excitation beam:

$$\mathbf{Plot[\delta e[2.311, \theta, 39.0] - 22.4, \{\theta, \theta min[2.311], \theta max[2.311]\}, AxesLabel \rightarrow \{"\theta", "\delta e"\}];}$$

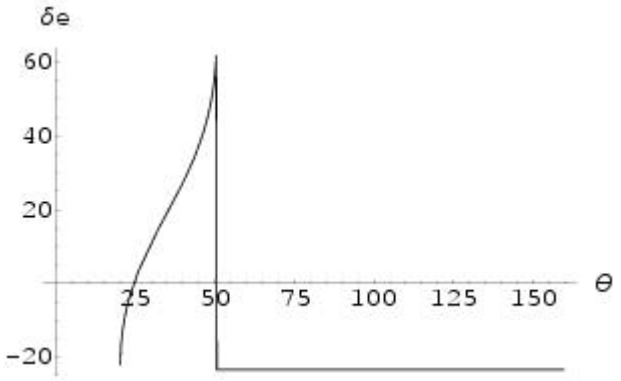

It looks like the solution is around θ=25 degrees:

$$\mathbf{x = Replace[\theta, FindRoot[\delta e[2.311, \theta, 20.45] == 22.4, \{\theta, 25\}]]}$$

$$\mathbf{\psi min[2.311, x]}$$

$$\mathbf{\psi max[2.311, x]}$$

25.0735

−0.216952

53.4821

Again, the crystal cut angle (20.45) is within the allowed range (-0.2, 53.5). The orientation for phase-matching will be:

$$\mathbf{\gamma 2[2.311, x, 20.45]}$$

0.644319

The direction of the output (upconverted) beam will be:

$$\mathbf{\gamma 3[2.311, x, 20.45]}$$

8.51803

The direction of the other input beam will be:

$$\mathbf{\gamma 1[2.311, x, 20.45]}$$

23.0443

Here's a plot of $\gamma 2$ vs a range of values of δ, for 2311 nm wavelength and 20.45 degree crystal cut angle:

$$\mathbf{Plot[\gamma 2[2.311, Replace[\theta, FindRoot[\delta e[2.311, \theta, 2.311] == x, \{\theta, 25\}]], 20.45], \{x, 19, 25\}, AxesLabel \rightarrow \{"\theta", "\gamma 2"\}];}$$

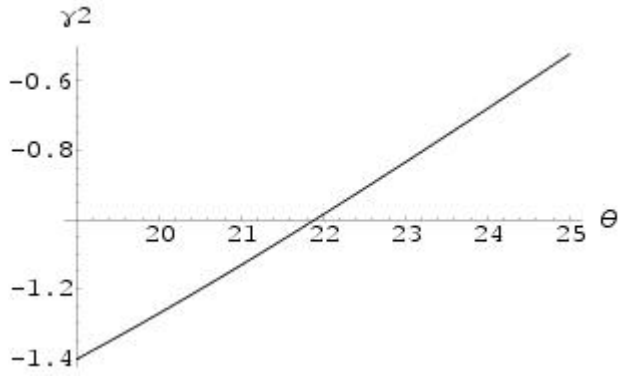

Bibliography

1. "https://ewhdbks.mugu.navy.mil/EO-IR.htm".
2. "http://www.as-photonics.com/SNLO".
3. APE, 163-165 Haus N 13053 Berlin Germany. *APE OPO PP Automatic Manual: Synchronously Pumped OPO*. URL `www.ape-berlin.com`.
4. Bartak, John R. *Mitigating the MANPADS Threat: International Agency, U.S., and Russian Efforts*. Master's thesis, Naval Postgraduate School, 2005.
5. Chirsto, Farid C. "Thermochemistry and Kinetics Models for MagnesiumTeflon/Viton Pyrotechnic Compositions". DSTO-TR-0938, 1999.
6. Coherent Laser Group, 5100 Patrick Henry Drive Santa Clara, CA 95054. *Operator's Manual The Coherent Mira Model 900-F Laser*.
7. Cooley, William T. *Measurement of Ultrafast Carrier Recombination Dynamics in Mid-Infrared Semiconductor Laser Material*. Ph.D. thesis, Air Force Institute of Technology (AETC), 1997.
8. Cumblidge, Kevin. *Using Time-Resolved Photoluminescence to Measure the Excitation and Temperature Dependence of Carrier Relaxation in Mid-Wave Infrared Semiconductors*. Master's thesis, Air Force Institute of Technology (AETC), 2004.
9. Freese, Thomas A. "Force Protection and Strategic Air Mobility: The MANPAD Challenge", 1999.
10. Gorski, Steve. *Carrier Dynamics in Mid-Infrared Quantum Well Lasers Using Time-Resolved Photoluminescence*. Master's thesis, Air Force Institute of Technology (AETC), 2002.
11. Iiams, Kevin M. "The MANPAD Threat to Civilian Airliners". USAWC Strategy Research Project.
12. Johnson, Peter. *Deviation of Time-Resolved Luminescence Dynamics in MWIR Semiconductor Materials From Carrier Recombination Theory Predictions*. Master's thesis, Air Force Institute of Technology (AETC), 2004.
13. Knowles, John. "Infrared Countermeasures". *PC Magazine*, 2003.
14. Mahr, H. and M. D. Hirsch. "An Optical Up-Conversion Light Gate with Picosecond Resolution". *Optics Commumication*, 13(2):96–99, February 1975.
15. McKelvey, John P. *Solid State Physics for Engineers and Material Science*. Krieger Publishing Company, 1993.
16. Mica, John. "H.R. 4056 [108th]: Commercial Aviation MANPADS Defense Act 2004". 108th Congress, 2nd Session, March 30 2004.
17. Office", "United States General Accounting. "Electronic Warfare: DoD Should Select Most Cost-Effective Infrared Countermeasure System". GAO/NSIAD-98-2.

18. van Ovost, Jacqueline D. "Global Mobility: Anywhere, Anytime, Any Threat? Countering the MANPADS Challenge". Occasional Paper No. 38 Center for Strategy and Technology Air War College.

19. Pretsch, Rogor A. "The Key to Defeating the Army After Next: Man-Portable Air Defense Systems Against the Air-Mechanized Formation". Monograph regarding the Army After Next Concept.

20. Roberts, Peter C. *Measurement of Carrier Dynamics in Mid-Infrared Semiconductors with Sub-Picosecond Resolution*. Ph.D. thesis, Air Force Institute of Technology (AETC), 2006.

21. Saleh, Bahaa E. A. and Malvin Carl Teich. *Fundamentals of Photonics*. Wiley-Interscience, 2007.

22. Shah, Jagdeep. "Ultrafast Luminescence Spectroscopy Using Sum Frequency Generation". *IEEE Journal of Quantum Electronics*, 24(2):276–288, February 1988.

23. Valentin G. Dmitriev, Gagik G. Gurzadyan and David N. Nikogosyan. *Handbook of Nonlinear Crystals*. Springer, 1997.

24. Verdeyen, Joseph T. *Laser Electronics*. Prentice Hall, 1995.

25. Whitmire, James C. "Shoulder Launched Missles (A.K.A MANPADS)". Paper No. 37 of the Counterproliferation Paper Series from the USAF Counterproliferation Center.

REPORT DOCUMENTATION PAGE

Form Approved
OMB No. 0704-0188

PLEASE DO NOT RETURN YOUR FORM TO THE ABOVE ORGANIZATION.

1. REPORT DATE *(DD-MM-YYYY)*	2. REPORT TYPE	3. DATES COVERED *(From - To)*
27-03-2008	Master's Thesis	June 07 - March 08

4. TITLE AND SUBTITLE

Ultrafast spectroscopy of mid-infrared semiconductors using the signal and idler beams of a synchronous optical parametric oscillator

5a. CONTRACT NUMBER

5b. GRANT NUMBER

5c. PROGRAM ELEMENT NUMBER

6. AUTHOR(S)

Derbis, Richard M., Captain, USAF

5d. PROJECT NUMBER

5e. TASK NUMBER

5f. WORK UNIT NUMBER

7. PERFORMING ORGANIZATION NAME(S) AND ADDRESS(ES)

Air Force Institute of Technology
Graduate School of Engineering and Management (AFIT/EN)
2950 P Street, Building 640

8. PERFORMING ORGANIZATION REPORT NUMBER

AFIT/GAP/ENP/08-M02

9. SPONSORING/MONITORING AGENCY NAME(S) AND ADDRESS(ES)

Intentionally left blank

10. SPONSOR/MONITOR'S ACRONYM(S)

11. SPONSOR/MONITOR'S REPORT NUMBER(S)

12. DISTRIBUTION/AVAILABILITY STATEMENT

APPROVED FOR PUBLIC RELEASE; DISTRIBUTION UNLIMITED.

13. SUPPLEMENTARY NOTES

14. ABSTRACT

The objective of this thesis was to improve the procedure for taking ultrafast, time-resolved measurements of photoluminescence from MWIR semiconductors. Previous work has used a mode-locked titanium sapphire (Ti:Saph) laser to excite the semiconductor sample and to upconvert the photoluminescence from the semiconductor. Work completed in this thesis improved on the techniques developed during previous work. A synchronous Optical Parameter Oscillator (OPO) will be used to convert the Ti:Saph laser 0.830 micron into 1.3 micron signal and 2.3 micron idler beams. Whereas the Ti:Saph reference and signal beams were too energetic to excite the quantum well (QW) layers of certain MWIR opto-electronic semiconductor structures, the synchronous OPO allows investigation of the active layer by directly exciting the QWs. Photoluminescence was detected from an indium arsenide antimonide (InAsSb) sample with a peak wavelength of 3.8 micron. A detailed procedure for setup of the TRPL experiment using the synchronous OPO is provided.

15. SUBJECT TERMS

Carrier dynamics, photoluminescence, mid-infrared semiconductor lasers, InAsSb, TRPL

16. SECURITY CLASSIFICATION OF:			17. LIMITATION OF ABSTRACT	18. NUMBER OF PAGES	19a. NAME OF RESPONSIBLE PERSON
a. REPORT	b. ABSTRACT	c. THIS PAGE			Michael A. Marciniak, ENP
U	U	U	UU	54	19b. TELEPHONE NUMBER *(Include area code)* (937) 255-3636, ext 4529

Reset

Standard Form 298 (Rev. 8/98)
Prescribed by ANSI Std. Z39.18